Received: 7 October 2022 | Accepted: 17 November 2022

DOI: 10.1002/pamm.202200200

MHD flow of submerged jets behind the inlet disturbance

Dmitry Krasnov[1], **Yaroslav Listratov**[2,3,*], **Ivan Belyaev**[2,3], **Yuri Kolesnikov**[1], **Evgeny Sviridov**[2,3], and **Oleg Zikanov**[4]

[1] Technische Universität Ilmenau, PF 100565, 98684 Ilmenau, Germany
[2] Moscow Power Engineering Institute, 14 Krasnokazarmennaya Street, Moscow 111250, Russia
[3] Joint Institute for High Temperature RAS, Izhorskaya 13 Bd.2, 125412, Moscow, Russia
[4] University of Michigan - Dearborn, 4901 Evergreen Road, Dearborn, MI 48128-1491, USA

In a broad variety of configurations in technology and industrial applications, the properties of liquid metal flows subjected to strong magnetic fields, are largely governed by the dynamics of coherent structures, known to settle several basic types, such as thin shear layers, forming near the walls or within the fluid domain, vortices extended along the field, or planar and round jets. In some cases, these structures are created by the design, like a submerged jet formed by a sudden expansion from the nozzle into a blanket channel, or jets formed behind some flow obstruction. In the other cases this may be due to instability and evolution of secondary structures, for example, descending and ascending jets appearing as a result of convective instability in blanket channels. In this study, we undertake an attempt to affect liquid metal flow via inlet disturbance formed by a simple rod placed along the magnetic induction lines. The disturbance can generate flat jets behind the rod and, furthermore, a sustainable flow of anisotropic vortical perturbations further downstream the flow. We seek to analyze the most important mechanisms of the flow dynamics and effects of magnetic field on the integral system properties of enhancing mixing, mass and heat transport for such flow. The most optimal regimes of vortex generation are found to be governed by the magnetic interaction parameter (Stuart number). The exact ratio of the optimal Stuart number is found to be in a range between 20 and 40, based on the channel double width as a characteristic size. The observed vortices attain quasi-2D shape and exist at a length of dozens of duct calibers, being the strongest at higher flow rates. The obtained flow regimes and their turbulent properties are also found to resemble significant similarity to the results on quasi-2D turbulence found in prior studies of channel and duct flows under spanwise magnetic field.

1 Introduction

One of the key effects, produced by the imposed magnetic field on the flow of conducting fluid, is suppression of turbulence. This, however, does not always lead to the development of laminar steady-state flows. The main reason is that the typical values of non-dimensional control parameters, such as Reynolds or Rayleigh numbers, are quite large in many liquid metal systems as, for example, in a fusion reactor blanket or a continuous steel casting facility. In these conditions, the flows – instead of getting laminar – may exhibit a very particular behavior with quasi two-dimensional (Q2D) instabilities, even at very strong magnetic fields. A typical outcome of these instabilities is the development of large-scale, Q2D coherent structures dominating the flow dynamics, such as shear layers, vortices, and jets anisotropically stretched along the magnetic field lines. These anisotropic structures often become unsteady due to the mechanism of Kelvin-Helmholtz instability, which leads to high-amplitude fluctuations of velocity, pressure, and temperature [1].

Another important feature of MHD flows is formation of thin internal and boundary shear layers, which also tend to be unstable. The intrinsic anisotropy of Q2D structures can profoundly modify the properties of both heat and mass transfer, leading to formation of stagnation zones, regions of reversed flow, localized hot and cold jets, anomalously strong fluctuations of temperature, rapidly changing stresses in the walls, etc. Particularly important and interesting are the jet flows found in various technological applications, for example in geometries with sudden expansions, in flows around obstacles, or in mixing, heating or cooling in heat exchangers. Jet dynamics in a strong magnetic field can generate Q2D vortex structures developing downstream and, therefore, strongly affecting the flow properties.

Numerical simulations of time-dependent MHD flows, produced by the vortex generators, are often complicated due to high resolution demands, needed to properly address the extremely thin MHD boundary layers and – especially in case of still pronounced flow dynamics – the bulk region as well. In the context of vortex promotion these limitations, typical for a fully 3D simulation, can to some extent be overcome by applying 2D settings. This view is suggested by the results in [2], indicating that at strong magnetic fields the overall complexity of the problem collapses essentially to Q2D solutions. Further numerical studies have also shown that vortex promotion in MHD duct flows can indeed be highly effective.

In particular, it has been shown numerically in [3] that downstream mixing, generated by a cylinder wake (past a circular cylinder in a rectangular duct) under strong transverse magnetic field, can increase heat transfer by more than a factor of two in some cases. Transition from steady to unsteady flow regimes has been found to depend on the Hartman number and blockage ratio – the occlusion of the duct by the inner body. It was also shown in [4] that the magnitude of the local Nusselt number distribution scaled up with the Reynolds number and blockage ratio. At the same time, the maximum change in heat transfer

* Corresponding author: email yaroslav.listratov@gmail.com

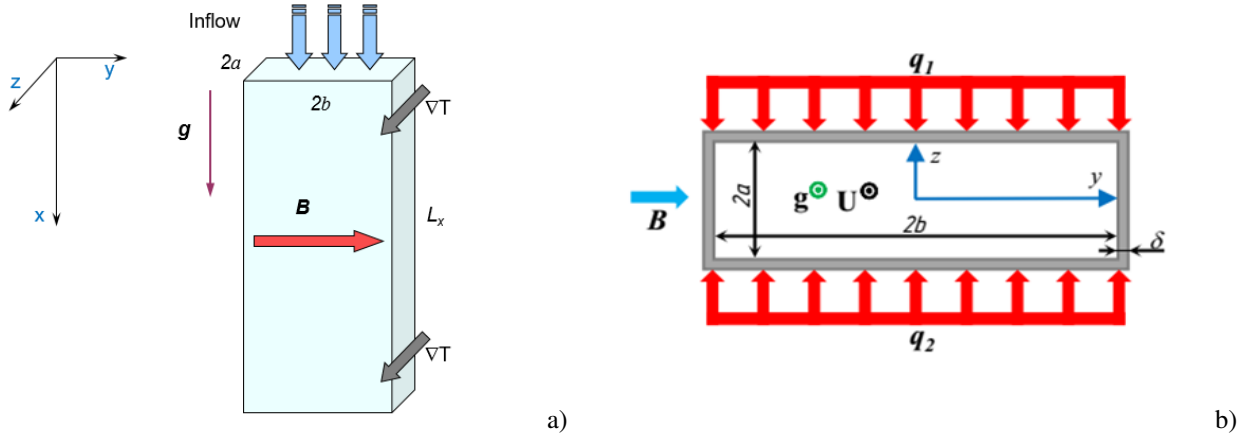

Fig. 1: Presentation of the problem **a** and the cross-section **b** of the flow

was found to be rather independent of the Reynolds number for small blockage ratios. A regression fit, which describes the decay of stable wake of vortices behind an idealized turbulence promoter (i.e., a circular cylinder) in a rectangular duct, was found in [5]. The model suggested that the decay rate varies with the blockage ratio, intensity of the imposed magnetic field, and Reynolds number.

Numerical studies also have identified regimes where secondary vortices, generated in Shercliff layers (i.e., boundary layers at the walls parallel to the magnetic field direction) and confined at the side walls, interact with the Karman vortices [6]. The increase of thermal efficiency of vortex promotion in an MHD duct flow, caused by introduction of a single cylinder, has been estimated in [7]. From a practical engineering viewpoint, a substantially beneficial gain in thermal efficiency versus the corresponding empty channel has been found near 30%. Recent studies on the influence of the shape of vortex promoters have shown that at conditions, relevant to fusion applications, the triangular object performs better than the circular and square cylinders [8]. However, there still is a lack of information on the actual performance of vortex promoters in experimental conditions close to the real use in industrial applications.

2 Materials and Methods

In this work, we study the downward flow of liquid metal in a rectangular channel (Fig. 1a). The results, discussed below, are obtained as a collaborative effort involving numerical simulations and experimental measurements.

2.1 Experimental method

Experiments are performed using the HELMEF facility (HELMEF) described in [9]. The model fluid is a liquid mercury circulating in a closed loop. The flow is driven in the streamwise x-direction by a pump. The imposed magnetic field B has the dominant spanwise component along the y-direction. The main part of the experimental test section has a rectangular cross-section (see Fig. 1) of the inner dimensions $2a \times 2b = 56 \times 16$ mm, with the walls made of stainless steel (AISI 316) of $\delta = 2$ mm thickness. Heating of the test section is provided by two independently controlled flat nichrome heaters, attached at longer sidewalls (Fig. 1b).

The experimental test section (Fig. 2a) was placed inside an electromagnet, which can create a magnetic field of up to 1.8 T within an 80 mm gap. The test section contains an input chamber, honeycomb, section with flow vortex promoter, the main part with the plate heaters and diagnostic sensors attached, the exit chamber, and the immersion measuring probe. The entry region of the flow (see the "aux. section" in Fig. 2a) is meant to form the disturbance pattern formed by a simple rod, placed along the long side of the duct (Fig. 2b). The distance between the axis of the rod and the measurement section is 790 mm and this entire length is assumed to be an area of a uniform magnetic field.

In the experiments, immersion sensors of two types have been used. The first one is a probe with single K-type thermocouple (hot junction diameter 250 μ). The second one is a special articulated probe consisting of two K-type thermocouples located in a plane perpendicular to the magnetic field lines. The distance between the thermocouples was 3.4 mm. This probe serves a dual purpose, as it allows simultaneous measurement of the flow temperature at two points of the cross-section and the longitudinal component of the flow velocity as a conductive velocity sensor. Measurements of the velocity field using potential probe method in case of non-isothermal flow are complicated because of the added complexity of corrections for thermoelectric effects in potential measurements [10].

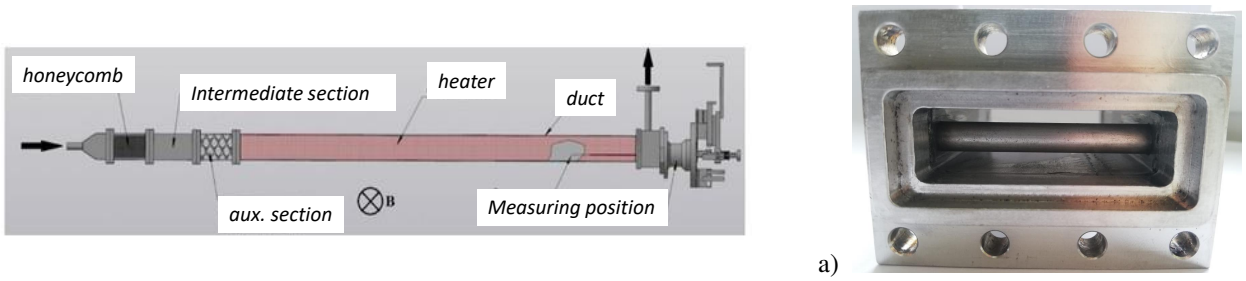

Fig. 2: Configuration of the experimental test section **a** and the inlet disturbance **b**, placed past the honeycomb. A uniform spanwise magnetic field B is applied to the duct over its longer side. Cylinder rod with $d = 8\,\text{mm}$ is parallel to the applied magnetic field and perpendicular to the main flow, blocking about 50% of the cross-section

2.2 Numerical and physical model

We consider the liquid metal ($Pr = 0.0025$ – typical for mercury) flow in a rectangular duct. The physical model we assumed is a non-isothermal and incompressible flow of an electrically conducting fluid with constant physical properties. The computational domain stands for a long rectangular duct with non-dimension size $32\pi \times 7 \times 2$ in, correspondingly, streamwise *x*-, spanwise *y*- and transverse *z*- directions. The length of the computational domain stretches quite far downstream and is certainly sufficient to simulate the experimental test section, while preserving the jet dynamics without possibly being impacted by the outlet boundary conditions.

The disturbance was simulated using the blocking area of $8\,\text{mm} \times 56\,\text{mm}$ overlapping the inlet section in the middle, whereas the remaining "unblocked" gaps were prescribed laminar flat-duct profiles. This double-jet inlet, with flat jets specified at the sidewalls, is meant to mimic the flow pattern formed behind the long rod used in the experiments. A spatially uniform and time-independent spanwise magnetic field $\mathbf{B}\,\{0, B_y = B_0, 0\}$ has been imposed in the flow domain. We apply the quasi-static MHD approximation [11], which implies no induced magnetic field $\mathbf{b}$. Also, for flows with heat transport we use the Boussinesq approximation for the buoyancy force. Both of these are a commonly used approximation, typically valid for liquid metal MHD flows in a broad range of parameters. The governing equations are non-dimensionalized using the duct half-width a as the length scale, mean streamwise duct velocity U_0 as the velocity scale, aU_0B_0 as the scale of electric potential, where B_0 is the magnetic field strength and qa/λ as the scale for the temperature θ calculated relative to the entrance temperature T_o, where $q = (q_1 + q_2)/2$ is the long-wall-averaged rate of non-uniform duct heating. The equations take the following form:

$$\frac{\partial \mathbf{u}}{\partial t} + (\mathbf{u}\cdot\nabla)\mathbf{u} = -\nabla p + \frac{1}{Re}\nabla^2\mathbf{u} + Ha^2Re^{-1}\mathbf{j}\times\mathbf{e}_b + GrRe^{-2}\theta\times\mathbf{e}_g, \tag{1}$$

$$\nabla\cdot\mathbf{u} = 0, \tag{2}$$

$$\frac{\partial \theta}{\partial t} + (\mathbf{u}\cdot\nabla)\theta = -\nabla p + \frac{1}{RePr}\nabla^2\theta, \tag{3}$$

$$\mathbf{j} = -\nabla\phi + \mathbf{u}\times\mathbf{e}_b, \tag{4}$$

$$\nabla^2\phi = \nabla\cdot(\mathbf{u}\times\mathbf{e}_b), \tag{5}$$

where $\mathbf{e}_g$ is the unit-length vector in the direction of gravity and $\mathbf{e}_b$ is the non-dimensional vector of imposed magnetic field.

The non-dimensional parameters of the problem (1-5) are the Reynolds number $Re = U_0a/\nu$, the Prandtl number $Pr = \nu/\chi$, the Hartman number $Ha = B_0a\sqrt{\sigma/\rho\nu}$ or Stuart number $N = Ha^2/Re$ and the Grashof number $Gr = g\beta q(4a)^4/\lambda\nu^2$, where g is gravitation and β, ν, ρ, σ, λ, χ stand, correspondingly, for the thermal expansion, kinematic viscosity, density, electric and thermal conductivity, and diffusivity of the fluid.

The boundary conditions for velocity at solid walls are those of zero slip. The convective outflow condition $\partial\mathbf{u}/\partial t + U_0\partial\mathbf{u}/\partial x = 0$ is applied at the exit of the domain. The inlet velocity in the unblocked inlet areas is directed along the channel and is given by parabolic profiles.

The problem is solved using the conservative finite-difference scheme of the second order on a structured collocated grid. Its accuracy and efficiency in simulations of high Ha flows is demonstrated, e.g., in [11]. The simulations are conducted on a computationalthe grid of $7200 \times 512 \times 128$ points, which is uniform in the streamwise *x*-direction and non-uniform in the wall-normal *y*- and *z*-directions. In order to account for electric conductivity of the walls and the uncertain effect of the contact resistance, simulations are performed for electrically perfectly insulating walls and walls of finite conductance ratio in the thin-wall approximation.

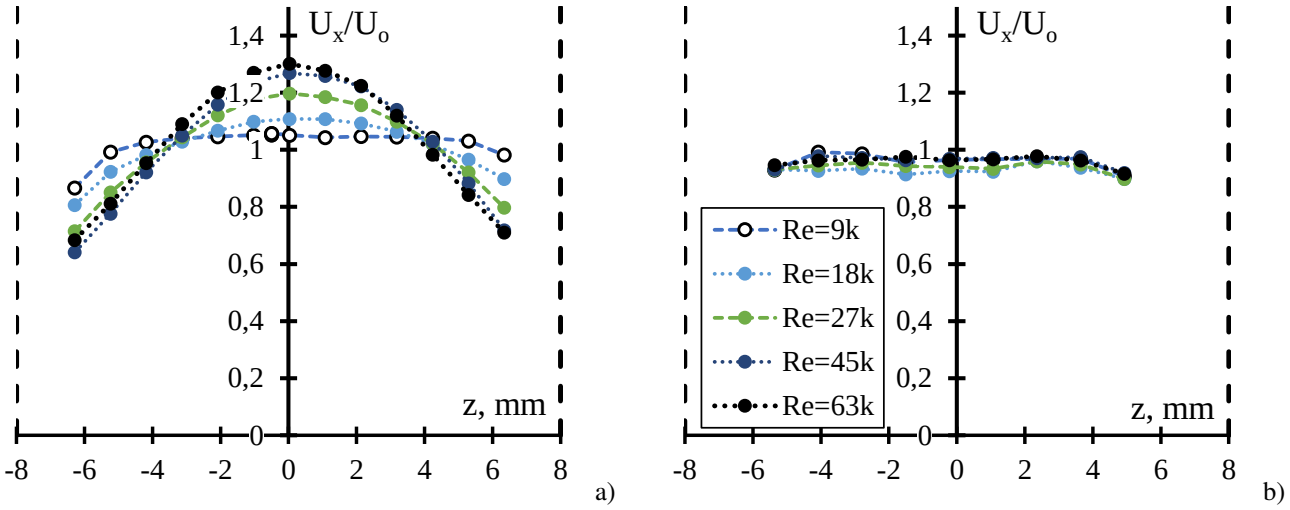

Fig. 3: Velocity profile measured at $x = 99a$ and $y = 0$ from the inlet at Ha=1300: **a** - without inlet disturbance; **b** - with inlet disturbance

3 Results and discussion

An experimental study has shown that the inlet device, built into the duct, can significantly change the flow parameters. Its application in the model experiments did not cause any difficulties associated with the construction part, which looks optimistic for real applications and/or practice. In that way, the inlet flow unit can generate sustainable flow perturbations by a cylinder rod aligned with the magnetic field induction lines. Optimal regimes with vortex production – quantified as RMS-velocity fluctuations – are found to be governed by the Stuart number N. The exact ratio of the optimal Stuart number is found to be in a range between 20 and 40, based on the double duct-width. In the observed flow regimes, vortex patterns existed at a length of dozens of duct calibers, being strongest at higher flow rates. The reliability of the experimental findings is also confirmed by the results of DNS, performed for a selected range of parameters. In particular, the phenomenon of a steeper velocity profile, observed in experiments (Fig. 3), is also found and confirmed by DNS (shown in Fig. 4a), with the relative difference not exceeding $4 - 5\%$.

It should be stressed that similar results for the mean velocity profile getting steeper have been observed in prior studies of turbulent duct and channel flows under spanwise magnetic field ([12], [11]). This particular trend has been associated with the formation of anisotropic, e.g., Q2D flow at strong magnetic fields. These findings clearly call for a deeper and thorough analysis of this type of flows and the associated local and global properties, including the transport processes, with the numerical simulations. It will allow one to study, for example, the characteristics and structures immediately near the wall, such as strong modification of the turbulent log-layer, shown in Fig. 4(b). Obviously, this non-trivial and non-standard near wall behavior is expected to affect mass and heat transport processes as well as integral parameters, such as the global friction coefficient C_f.

Generated vortices, as shown in Fig. 5 for $Re = 63000$ and $Ha = 1300$, can efficiently alter the naturally evolving magneto-convective secondary structures, decreasing the amplitude and irregularity of temperature fluctuations or even completely diverting them. The induced vortices strongly modify the flow structure due to the development and transport of Q2D perturbations, which can sufficiently enhance heat transfer. In some cases, explored here, the integral heat transfer is found to be as twice as more effective, which is of interest for practical application, even outside the context of superseding natural flow fluctuations evolving at high thermal load.

4 Conclusions

As an outlook for possible directions of the future study, a few important points should be mentioned here. First of all, the study will be continued with its main focus on the mechanisms of heat transfer, interacting with (or affected by) the strong Q2D structures due to the vortex promoters. At this point, several sizes of the inlet disturbances as well as their effect on the specific pattern formation, flow anisotropy and temperature fluctuations can be explored.

Secondly, the discovered phenomena should further be explored with numerical simulations, performed at higher resolution and more systematically, covering a broader range of flow regimes. This would allow a more accurate and detailed assessment of the flow parameters and the properties of strongly anisotropic MHD flow states.

Finally, the experimental study will be continued with an improved set of acquisition sensors, which would allow much finer spatial resolution - an aspect, particularly important in the close proximity to the walls. That way both the experimental and numerical findings can be compared over the entire cross-section of the duct, and this can also serve an additional

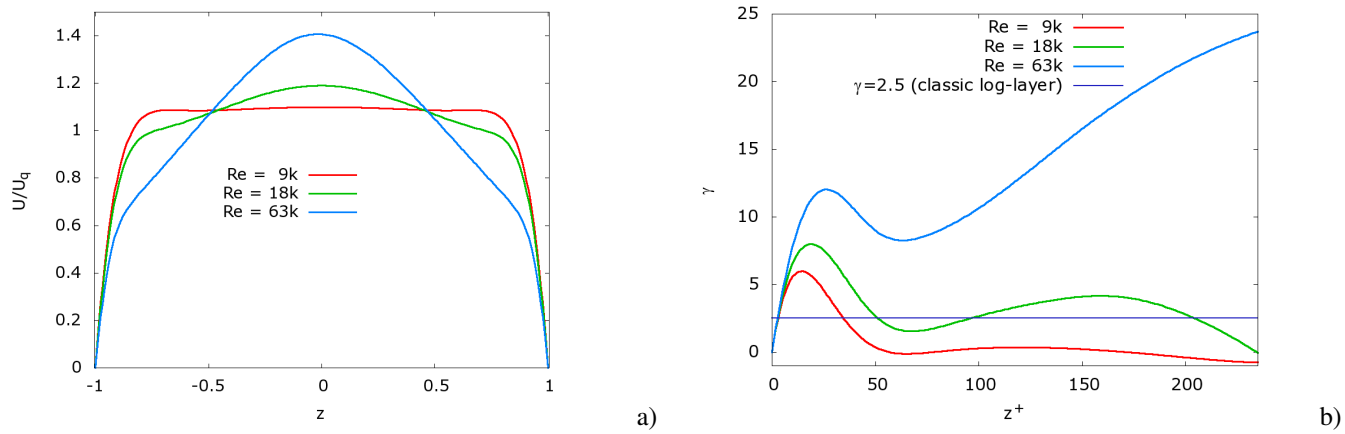

Fig. 4: Results of DNS on the basic velocity profiles $U(z)$ at $Ha = 1300$ and $Re = 9000, 18000$ and 63000, visualized at $y = 0$ and $x = 99a$ (as in experiment) and averaged over 20 convective time units for fully developed flow states. Shown are: **a** - velocity profiles $U(z)$ and their modification due to effect of the spanwise magnetic field B_y in channel units and **b** - compensated velocity gradients $\gamma = z^+ dU^+/dz^+$ in wall-units. The wall-units, as commonly accepted in the literature, are calculated based on the duct half-height as the length-scale, and the values of shear-based Reynolds number $Re_\tau = u_\tau a/\nu$ obtained in DNS as: 170 (at $Re = 9000$), 235 (at $Re = 18000$) and 400 (at $Re = 63000$)

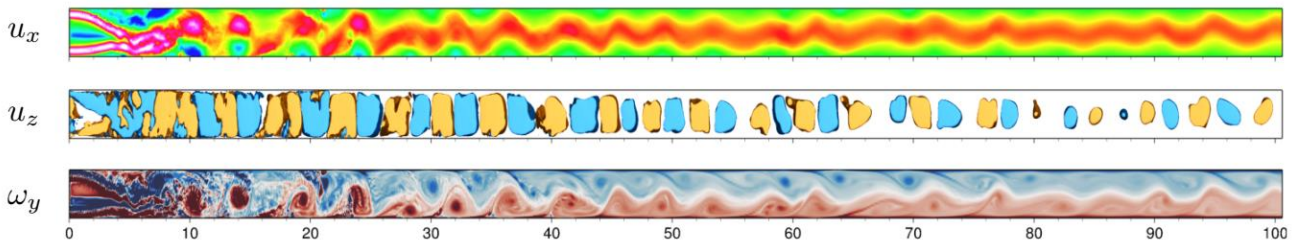

Fig. 5: Results of DNS at $Ha = 1300$ and $Re = 63000$, performed in the domain with streamwise length $L_x = 32\pi$. Instantaneous snapshot of a fully developed flow state after 100 convective units of the temporal evolution is shown in the *(x,z)*-mid-plane at $y = 0$. Visualized are: isocontours of the streamwise velocity u_x (top subplot), iso-surfaces of the vertical velocity $u_z = \pm 0.1$ (middle subplot) and spanwise vorticity component ω_y (bottom subplot). The uniform magnetic field B_y is normal to the shown *(x,z)*-planes, the x-coordinate has been rescaled by a factor of $1/2$ to facilitate better visibility

cross-validation and verification of the both approaches. Some of these points raised above are directly associated with the applications aspects, aimed to enhance or suppress mass and heat transport in a certain direction, an asset seen important in industrial systems. The others are more relevant to the fundamental questions of wall-bounded Q2D MHD turbulence, e.g., the structure and behavior of the MHD boundary layers under spanwise magnetic field. This could be very helpful for constructing proper turbulence models, thus, simplifying CFD analysis of the complex flow geometries, yet again typical for industrial applications.

Acknowledgements The work was supported by the award 20-69-46067 from the Russian Science Foundation and the basic experimental statement funded by the joint Russian–German collaboration program performed in 2018-2020 within research grants RFBR NNIOa 18-508-12005 and DFG KR 4445/2-1.

References

[1] O. Zikanov, I. Belyaev, Y. Listratov, P. Frick, N. Razuvanov, and V. Sviridov, Applied Mechanics Reviews **73**(1), 010801 (2021).
[2] B. Mück, C. Günther, U. Müller, and L. Bühler, Journal of Fluid Mechanics **418**, 265–295 (2000).
[3] W. K. Hussam, M. C. Thompson, and G. J. Sheard, International Journal of Heat and Mass Transfer **54**(5-6), 1091–1100 (2011).
[4] W. K. Hussam and G. J. Sheard, International Journal of Heat and Mass Transfer **67**, 944–954 (2013).
[5] A. H. Hamid, W. K. Hussam, A. Potherat, and G. J. Sheard, Physics of fluids **27**(5), 053602 (2015).
[6] M. Farahi Shahri and A. Hossein Nezhad, International Journal of Applied Electromagnetics and Mechanics **49**(1), 123–132 (2015).

[7] O. G. Cassells, W. K. Hussam, and G. J. Sheard, International Journal of Heat and Mass Transfer **93**, 186–199 (2016).
[8] W. K. Hussam, A. H. Hamid, Z. Y. Ng, and G. J. Sheard, International Journal of Thermal Sciences **134**, 453–464 (2018).
[9] I. A. Belyaev, V. G. Sviridov, V. M. Batenin, D. A. Biryukov, I. S. Nikitina, S. P. Manchkha, N. Y. Pyatnitskaya, N. G. Razuvanov, and E. V. Sviridov, Thermal Engineering **64**(11), 841–848 (2017).
[10] C. Fazio, Handbook on Lead-bismuth Eutectic Alloy and Lead Properties, Materials Compatibility, Thermal-hydraulics and Technologies: 2015 Edition - Introduction (OECD, Paris (France), 2016).
[11] D. Krasnov, O. Zikanov, and T. Boeck, J. Flud Mech. **704**, 421 (2012).
[12] D. Krasnov, O. Zikanov, J. Schumacher, and T. Boeck, Physics of fluids **20**(9), 095105 (2008).

